remote sensing

MDPI

Communication

Active Hyperspectral Scanning of Rock Face with a Supercontinuum Laser

Harald van der Werff [1,†], Christoph Hecker [1,*,†], Alfred Baines [2], Andries E. J. Botha [1], Joe Fletcher [2] and Bruno Portela [1]

[1] Faculty for Geo-Information Science and Earth Observation, University of Twente, 7522 NH Enschede, The Netherlands; harald.vanderwerff@utwente.nl (H.v.d.W.); a.e.j.botha@utwente.nl (A.E.J.B.); bruno.portela@utwente.nl (B.P.)
[2] Viridien Group, Crawley, West Sussex RH10 9QN, UK; alfie.baines@viridiengroup.com (A.B.); joe.fletcher@viridiengroup.com (J.F.)
* Correspondence: c.a.hecker@utwente.nl
† These authors contributed equally to this work.

Abstract: Underground environments present a challenge for hyperspectral outcrop analysis. In addition to operational safety and moisture, illumination is the main concern in data acquisition. We report a supercontinuum laser for illuminating rock faces in hyperspectral data acquisition. We present the early results of combining an off-the-shelf hyperspectral camera with a supercontinuum laser system, measured at night on rock faces in a former open-pit mine in southeast Spain as a proxy for underground lighting conditions. Band ratios specifically developed for this geological setting and low-light conditions highlight key minerals that can be used as a vector toward the ore zone. We successfully highlight the key indicator minerals and their distribution patterns for defining gold-bearing ore zones and that supercontinuum white laser light is a feasible illumination source for hyperspectral line scanners under field conditions.

Keywords: hyperspectral; low-light conditions; supercontinuum laser; illumination; mining; mineral mapping

check for updates

Citation: van der Werff, H.; Hecker, C.; Baines, A.; Botha, A.E.J.; Fletcher, J.; Portela, B. Active Hyperspectral Scanning of Rock Face with a Supercontinuum Laser. *Remote Sens.* **2024**, *16*, 4631. https://doi.org/10.3390/rs16244631

Academic Editor: Lenio Soares Galvao

Received: 28 October 2024
Revised: 29 November 2024
Accepted: 6 December 2024
Published: 11 December 2024

Copyright: © 2024 by the authors. Licensee MDPI, Basel, Switzerland. This article is an open access article distributed under the terms and conditions of the Creative Commons Attribution (CC BY) license (https://creativecommons.org/licenses/by/4.0/).

1. Introduction

The hyperspectral scanning of outcrop and rock faces in the field provides crucial mineralogical information for the mining industry [1]. The shortwave infrared wavelength region is key for mapping alterations in mineralogy [2] due to absorption overtones and combinations of their fundamental vibration energy modes that occur at longer wavelengths [3]. About 40% of the world's mines are underground [4]. In addition to limited accessibility, operational safety concerns, and abundant moisture in the air and on rock surfaces [5], providing adequate illumination in these underground conditions is a challenge. Kirsch et al. [1] studied underground acquisition conditions, including halogen light sources. Halogen lamps however consume a lot of power and produce heat, so are impractical in operational underground environments.

An alternative light source for spectroscopy is a supercontinuum laser [6]. The term supercontinuum refers to a set of nonlinear effects that broaden the spectral range of optical pulses. As the power of the input pulses increases, the extent of spectral broadening also increases, eventually covering the visible, near-infrared, and shortwave infrared wavelengths [7]. The light can be directed into a narrow beam with high irradiance at low energy consumption using a Powell lens. Supercontinuum lasers have been used in multispectral lidar (e.g., [8–10]), hyperspectral lidar (e.g., [11]), and as alternative broadband white light source in infrared spectroscopy [6,12]. Kääriäinen et al. [13] and Nischan et al. [12] used a supercontinuum laser for hyperspectral imaging.

We used a supercontinuum laser and a full-range hyperspectral camera with continuous wavelength coverage for rock face scanning in the field, which is the first time this has been conducted, to the best of our knowledge. We limited the experiment to off-the-shelf or commercially available hardware components for this proof of concept. This communication explains how the system was deployed to collect data from a former epithermal gold mine in southeastern Spain. By measuring real-world rock outcrops at night in an open-pit mine and along an access road, we simulated underground illumination conditions. The collected data demonstrate the ability of active illumination with a supercontinuum laser to differentiate key hydrothermally altered minerals with hyperspectral data.

2. Test Site and Data Acquisition

The Cabo de Gata volcanic field in southeast Spain was used as a test site. The area comprises two primary caldera complexes: Rodalquilar and Lomilla. Within the Rodalquilar caldera, two significant ore deposit types are present: low-sulphidation Pb-Zn-(Cu-Ag-Au) quartz veins, characterised by base metal sulphides within a quartz gangue, and high-sulphidation Au-(Cu-Te-Sn) ore, located in acid sulphate alteration zones on the eastern margin of the Lomilla caldera. Gold mineralisation occurs in two forms: primary gold, predominantly found in chalcedonic quartz veins and hydrothermal breccias, and secondary gold, which forms through the oxidation of primary sulphides and is associated with iron oxides and jarosite (Figure 1). The hydrothermal system exhibits zonations with depth, comprising a silicic zone characterised by vuggy silica and massive silicified rock associated with gold mineralisation; an advanced argillic zone containing alunite, diaspore, zunyite, and pyrophyllite; and an intermediate argillic zone consisting of quartz, kaolinite, illite, and minor alunite [14]. The alteration zones and accessible rock faces on the eastern margin of the Lomilla caldera provided an ideal setting for this proof-of-concept study.

Data were acquired from 7 to 12 April 2024. In this period, the humidity ranged from 40 % to 60 %, with no precipitation during the acquisition window or in the days prior. The cloud cover ranged from clear blue skies to partially cloudy conditions. The air quality was overall poor, with significant amounts of Sahara dust in the air. We measured outcrops under full daylight conditions (optimal situation), in twilight (low-light conditions assisted with laser light), and in complete darkness (with only laser illumination as a proxy for underground mine workings). Measurements at night were used as a proxy for underground mining conditions. We focused on identifying veins and pervasive alterations featuring spectrally active minerals, such as jarosite, alunite, kaolinite, and illite, to acquire images that highlight the typical spatial patterns of high-sulphidation deposits (Figure 1).

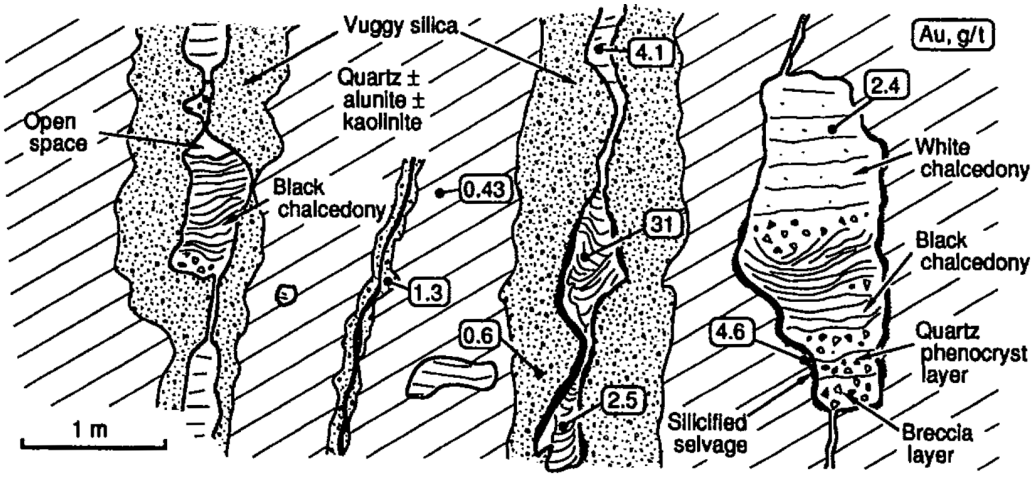


Figure 1. Schematic drawing of the chalcedony quartz veins and the interaction with the wall rock. The numbers indicate the gold contents [g/t] associated with the mineralogy. The figure is reused with permission from Arribas et al. [14].

3. Materials and Methods

3.1. Hardware

We used an off-the-shelf hyperspectral camera and supercontinuum laser system to test the suitability of a supercontinuum laser to illuminate rock faces for hyperspectral data acquisition.

The HySpex Mjolnir VS-620 (Norsk Elektro Optikk, Oslo, Norway) is a hyperspectral push-broom imaging system that acquires a hyperspectral data cube by scanning an outcrop from a horizontally rotating platform. The system consists of an S-620 shortwave infrared (SWIR) sensor with 620 spatial pixels and 300 spectral bands, a 5.1 nm sampling interval, a 20° (0.54 mrad/pixel) field-of-view, and a V-1240 visible and near-infrared (VNIR) sensor with 1240 spatial pixels and 200 spectral bands, 3 nm sampling interval, and a 20° (0.27 mrad/pixel) field-of-view. This system's lenses were optimised for a 22 m working distance.

The SuperK FIANIUM FIR-20 instrument (NKT Photonics, Birkerød, Denmark) is a class 4 laser that generates a supercontinuum light in the 490 to 2350 nm wavelength range [7]. A 30° Powell lens in a 1 inch lens holder was mounted on the collimator sleeve of the laser optical fibre cable to transform the laser point into a thin, vertical line. The laser fibre optic was mounted directly on the hyperspectral system (Figure 2). A rudimentary mount was assembled to align the laser beam with the instantaneous field of view of the SWIR detector. Both instruments were powered from a single 730 W h battery.



Figure 2. A photo of the hardware in daylight. The hyperspectral push broom camera is mounted on a tripod with a rotating head. The laser optical fibre and Powell lens are mounted on top of the camera. The active laser beam is visible as a bright yellow line on the rock face behind the camera.

3.2. Data Processing

Preprocessing was kept to a minimum to show the data as measured, which implied the data included noise resulting from low-light conditions and illumination artefacts originating from the fore-optics used. The raw HySpex data were converted to radiance-at-sensor values [$W\,m^{-2}\,sr^{-1}\,nm^{-1}$] utilising the supplier's software (HySpexRad v2.6). This software also corrected for smile and keystone distortion, which reportedly should be below 0.1 pixel [15]. The final step was a 90° rotation of the data from vertical to horizontal.

To target the diagnostic minerals jarosite, alunite, kaolinite and illite, we used data from the S-620 (SWIR) detector. Historical hand specimens from the open-pit mines were

newly measured in the GeoScience Laboratory of the University of Twente, using the same HySpex camera. In this setup, we used two 1000 W halogen spotlights from a 3 m distance for illumination. Based on the spectra obtained from this acquisition and prior knowledge of the mineral system and associated spectral absorption features, three band ratios were defined to highlight the described alteration mineralogy. The band ratios target the diagnostic spectral features of the alteration minerals by dividing the higher radiance values in the spectral shoulder by the lower radiance values in the central part of the absorption feature. This leads to high band ratio values for spectra that contain this particular spectral feature.

To preserve signal without needing to resample the data, the band ratios encompass multiple spectral absorption features, and the wavelengths selected as the numerator and denominator cover multiple spectral bands [16]. For jarosite, we targeted the left and right spectral slopes of the 2265 nm feature; for alunite, the left and right spectral slopes of the 1760 nm feature and the right slope of the 2170 nm feature; and, for kaolinite/illite, the left and right spectral slopes of the 2200 nm feature. A consequence is that band ratio 3 covers the largely overlapping 2200 nm spectral absorption features of both kaolinite and illite:

$$Jarosite = \frac{rad_{2042:2100}}{rad_{2247:2278}} + \frac{rad_{2298:2304}}{rad_{2247:2278}} \quad (1)$$

$$Alunite = \frac{rad_{1624:1659}}{rad_{1746:1781}} + \frac{rad_{1805:1833}}{rad_{1746:1781}} + \frac{rad_{2237:2295}}{rad_{2135:2210}} \quad (2)$$

$$Kaolinite/Illite = \frac{rad_{2042:2100}}{rad_{2193:2213}} + \frac{rad_{2247:2278}}{rad_{2193:2213}} \quad (3)$$

where rad is the mean radiance value for the spectral ranges defined in subscript [in nanometers]. These band ratios were applied to both daylight and laser-illuminated data.

4. Results

We show RGB (red-green-blue) colour composites of two different rock faces, covering the central ore zone in a quarry (Figure 3) and highly altered volcanic rocks in a nearby access road (Figure 4). The field photos (Figures 3a and 4a) show the outcrops with an indication of the section that was imaged by the hyperspectral camera. The true-colour RGB composites in Figures 3b and 4b are composed of VNIR radiance bands at 640 nm, 550 nm and 460 nm and show yellowish colouration due to the presence of jarosite, reddish to dark-brown colours due to the presence of hematite, and several patches of shadow are visible in black tones. False-colour RGB composites of SWIR radiance bands at 1650 nm, 1226 nm and 1026 nm are shown in Figures 3c and 4c for daylight results, and in Figures 3e and 4e for laser illumination. The RGB colour composites of band ratios acquired in daylight (Figures 3d and 4d) and with the laser (Figures 3f and 4f) indicate the presence of jarosite, alunite and kaolinite/illite in red, green and blue tones, respectively.

The data in Figure 3 were acquired at 14:34 Central European Time (CET) in daylight and at 19:30 CET in low-light conditions, from an approximately 10 m distance. With roughly equal amounts of remaining diffuse sunlight and added laser light, the average spectral radiance of the 19:30 image at a 1650 nm wavelength was roughly one-ninth of that in full daylight. In the band ratios, veins and patches of jarosite (red) and alunite patches (bright green) are easily distinguishable in the daylight and laser-illuminated data. A few bright blue patches visible in the daylight data are also in the centre of the laser-illuminated data but not at the bottom. Most pixels with blue tones (resulting from the kaolinite/illite ratio) also have mild reddish tones (from the jarosite ratio), giving a purplish hue to the image. The spatial patterns of the minerals in Figure 3d,f can be positively linked to the mineral distribution patterns reported for the ore zone in the literature (Figure 1).

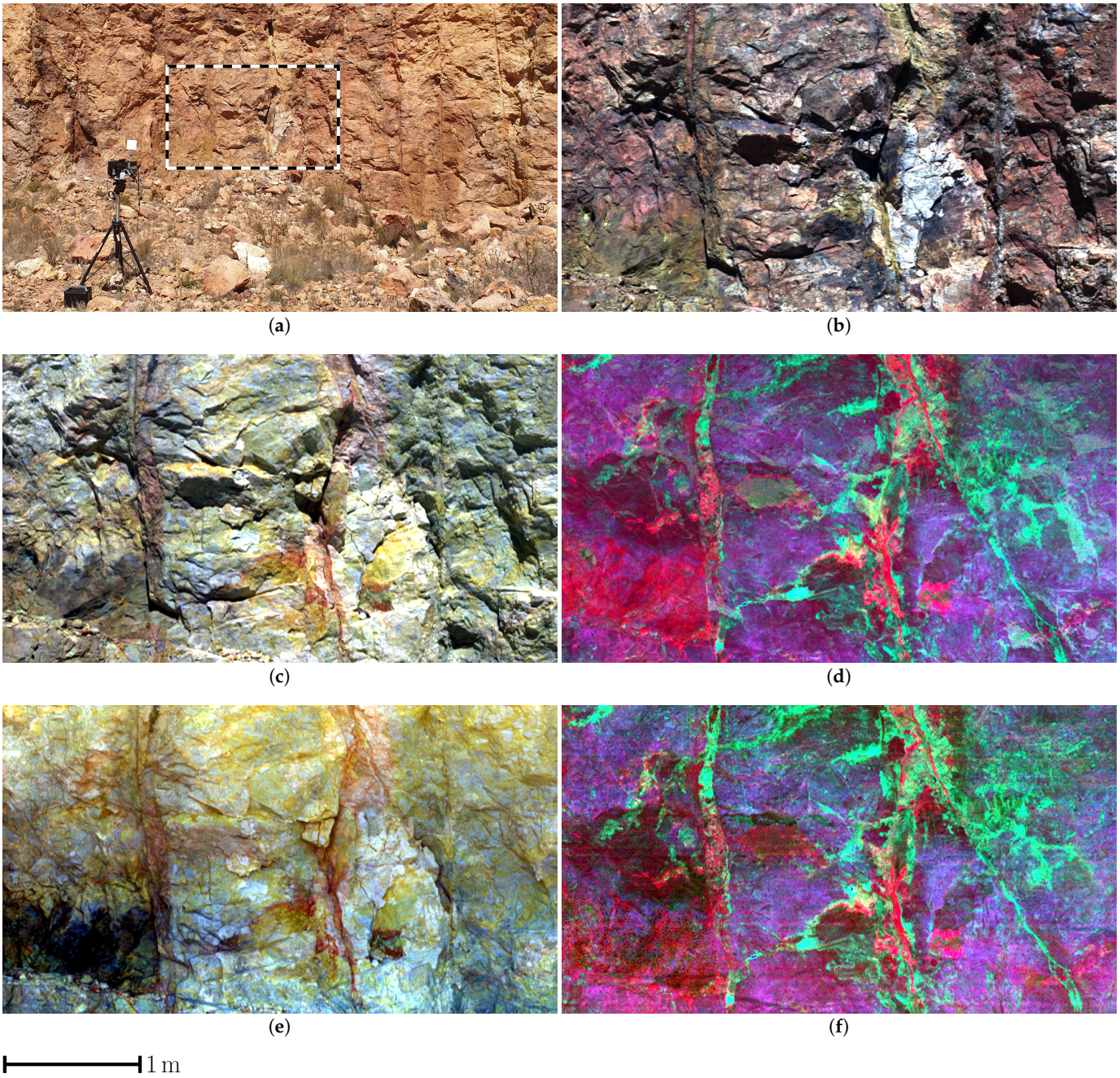


Figure 3. Band ratios of hyperspectral images acquired from a distance of 10 m in daylight (**b**–**d**) and in low-light conditions (**e**,**f**) illuminated with a supercontinuum laser. The photo taken in an open-pit mine shows the area imaged by the hyperspectral sensor with a dashed frame (**a**), the corresponding daylight true-colour composite in (**b**) and false-colour composite in (**c**). The daylight band ratios in (**d**) and low-light band ratio composite in (**f**) highlight, in a histogram equalisation stretch, the minerals jarosite (red; forming the central part of veins), alunite (green; forming the wider veins), and kaolinite/illite (blue to purple; pervasive alteration of the whole rock face). False-colour composites of laser-illuminated radiance bands at 1650 nm, 1226 nm and 1026 nm show a lack of shadows (**e**) when compared to the image acquired in daylight (**c**).

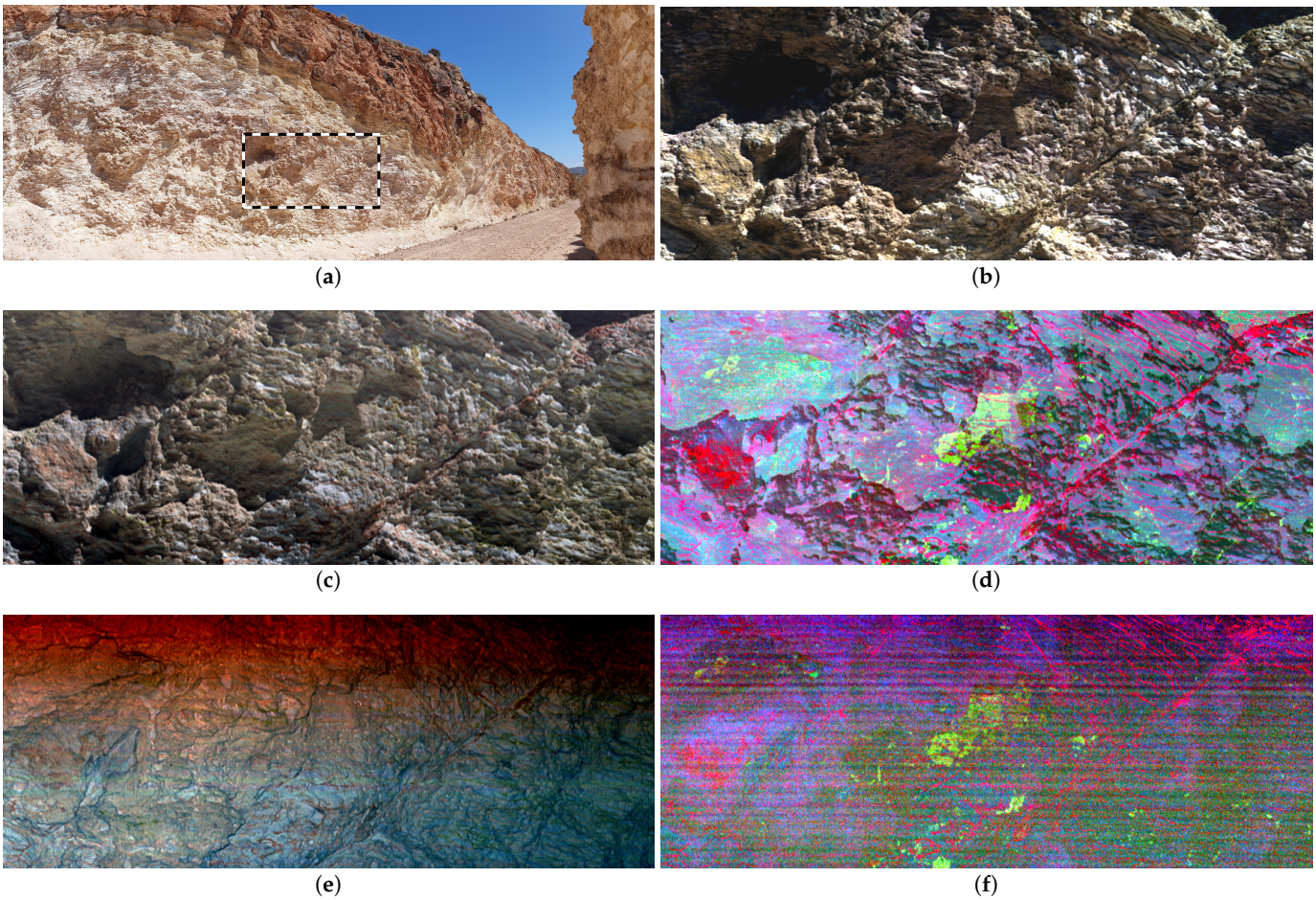


Figure 4. Band ratios of images acquired from a distance of 12 m in daylight (**b**–**d**) and in complete darkness (**e**,**f**) illuminated with a supercontinuum laser. A photo taken along an access road shows the area imaged by the hyperspectral sensor with a dashed frame (**a**), the corresponding daylight true-colour composite in (**b**) and daylight false-colour composite in (**c**). The daylight band ratios in (**d**) and darkness band ratio composite in (**f**) highlight jarosite (red veins), alunite (green patches), and kaolinite/illite (blue to purple; pervasive alteration of the whole rock face), which are shown in a histogram equalisation stretch. The false-colour composites of radiance bands at 1650 nm, 1226 nm and 1026 nm show a lack of shadows in the laser-illuminated image (**e**) when compared to the image acquired in daylight (**c**) but also a cross-track illumination difference between longer and shorter wavelengths.

The data in Figure 4 were acquired at 12:32 CET in full daylight and at 21:21 CET in complete darkness, from an approximately 12 m distance. The average spectral radiance at a 1650 nm wavelength for the 21:21 CET image was roughly one-fifth of that in daylight. The data acquired in daylight suffered from shadows and suboptimal illumination of the vertical wall, which explained the relatively small difference between the illumination sources. The data acquired with the laser in the dark suffered from along-track striping, but the veins with jarosite (red) and alunite patches (light green) nevertheless remained recognisable. The patches highlighted by dark green tones, however, changed considerably. This is an artifact of shadows that were present in the daylight data (Figure 4c) but not in the laser-illuminated data (Figure 4e). At the same time, Figure 4e shows a different distribution of laser light in the longer and shorter wavelengths, an artifact resulting from the Powell lens used to distribute the laser beam.

Figure 5 shows daylight and laser-illuminated radiance-at-sensor data reflected from a white panel at an approximately 12 m distance. The solar spectrum shows a typical

blackbody curve shape with water and carbon dioxide absorption features at ∼1150 nm, ∼1400 nm, ∼1900 nm and ∼2000 nm. The laser spectrum shows only weak atmospheric absorption features at ∼1400 nm & ∼1900 nm but has a peak at 1064 nm and a drop in signal at wavelengths above 2300 nm, a characteristic of this particular laser system.

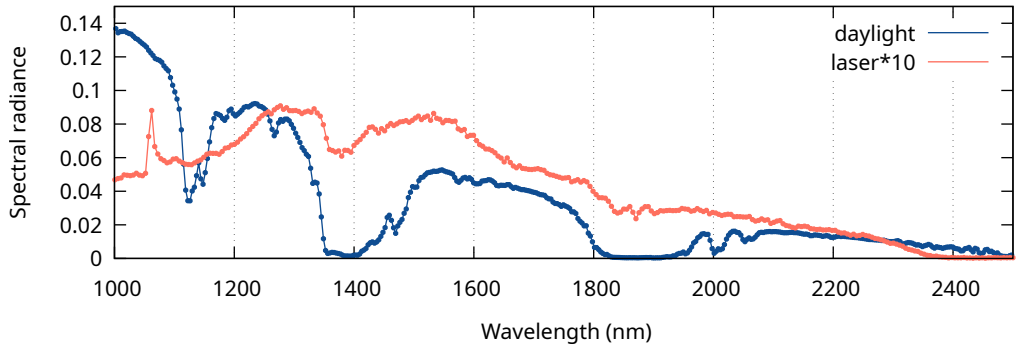


Figure 5. Radiance-at-sensor spectra [$W\,m^{-2}\,sr^{-1}\,nm^{-1}$] in the short-wave infrared, obtained by measuring a Spectralon® white panel (Labsphere, North Sutton, NH, USA) when illuminated by the sun in full daylight and by a supercontinuum laser in darkness. In the plot, the spectrum of the laser is enhanced by a factor of 10.

5. Discussion

The band ratios obtained with daylight and laser illumination (Figure 3) both reflect the presence and locations of gold-bearing veins in the ore zone of the Lomilla caldera (Figure 1). The results of the data acquired with the laser in low-light conditions are visually of comparable quality to those of daytime acquisition, having the same information highlighted (Figure 3d,f). Therefore, active hyperspectral scanning with a supercontinuum laser can, even with rudimentary means of attaching and aligning the laser source, successfully differentiate the major minerals that are used as vectors to the gold ore in this geological setting. Even with the Saharan dust present in the atmosphere, it was possible to discern minerals, indicating a potential for application of this system in underground mining atmospheres. We did not use any of the VNIR data acquired for mineral mapping; the minerals chosen to differentiate ore from gangue were all active in the SWIR. For other geological settings or mineralisations, both VNIR and SWIR could be required for analysis.

These results were achieved using band ratios specifically designed to show the spectral differences by incorporating multiple spectral bands to enhance the signal. A spectral or spatial filtering technique would be an alternative to increasing the signal. Still, filtering would come at a loss of spatial resolution or result in suboptimal resampling of spectral information. An added advantage of a knowledge-based definition of band ratios is that wavelengths affected by, e.g., atmospheric absorption still present in the laser-illuminated data, can be avoided.

As the signal under laser illumination is lower than under sunlight, some striping is currently contained in the images (Figure 4f). The low amount of light and slight calibration differences in the push broom detector array create along-track striping in the data. Destriping algorithms, a minimum noise fraction (MNF) transform, and a cross-track illumination correction were tested using ENVI 6.0 software. However, these added processing steps would primarily be needed to correct issues caused by our experimental setup. Improving the signal by shortening the measuring distance and improved alignment of the laser beam to the hyperspectral camera would likely make additional filtering techniques unnecessary. Even without optical or visual improvements, the results showed that filtering techniques were unnecessary to separate veins from gangue.

The different overall shape of the spectra is the reason that methods other than band ratios cannot easily be applied. In radiance-at-sensor data, vector-based similarity measures and feature-fitting approaches are hampered by spikes in the signal (Figure 5). Converting the radiance-at-sensor data to reflectance would allow comparison to reference spectra

and potentially result in (semi)quantitative information. We did not pursue this conversion given the suboptimal laser illumination throughout different wavelengths (Figure 4e). Characterization of the laser's illumination and subsequent correction could lead to reliable reflectance data and allow full-range similarity measures to be used. However, this application shows that conversion to reflectance is also not needed to differentiate ore from the surrounding rock. Our intended minimal processing approach demonstrates the feasibility of using radiance data to obtain action-ready information.

Differences in daylight and laser-illuminated band ratios result mainly from shadows in the daylight image (Figure 3c). The laser-illuminated image has, with the laser mounted directly on top of the camera, minimal shadows visible (Figure 3e). This gives active laser illumination an advantage over passive daylight illumination, which commonly is orientated at an angle to the measured surface, and requires complex corrections to enable quantitative spectral analysis [17]. An advantage of laser-illuminated acquisition over halogen light illumination is the power consumption. Where halogen spotlights or floodlights require multiple 500 W to 1000 W halogen lights and a matching power source, the laser can run from a dedicated battery for several hours.

The presented setup is straightforward, showing a comparative analysis of measurements acquired under solar and laser lighting conditions. The presented setup assumes that the width of the laser beam is sufficient for the instantaneous field of view of the camera's detectors and, in case data from multiple detectors are needed, that these detectors are sufficiently aligned. Experiments on scanning at different distances, with varying laser powers and wavelength coverages, application to differently angled and coloured rock surfaces, and, last but not least, operation in damp underground environments are needed to fully understand the applicability of supercontinuum lasers for mineral mapping in the field and in underground mines.

6. Conclusions

For the first time, we demonstrated that supercontinuum white laser light is a feasible illumination source for measuring rock faces in the dark. The laser beam can be combined and aligned with a hyperspectral line scanning camera on a rotation stage under field conditions, and the resulting images contain spectral information that can be used to successfully differentiate key hydrothermal alteration minerals known as a vector towards ore.

Author Contributions: Conceptualisation, C.H., H.v.d.W., A.B., A.E.J.B., J.F., and B.P.; methodology, C.H., H.v.d.W., A.B., A.E.J.B., J.F., and B.P.; software, H.v.d.W.; formal analysis, C.H., H.v.d.W., A.E.J.B., and A.B.; resources, J.F., A.E.J.B., and B.P.; data curation, H.v.d.W., A.E.J.B., and C.H.; writing—original draft preparation, H.v.d.W.; writing—review and editing, C.H., B.P., A.E.J.B., J.F., and A.B.; visualisation, H.v.d.W., and C.H.; project administration and coordination, A.E.J.B., and J.F.; Authors H.v.d.W., and C.H. contributed equally to this paper. All authors have read and agreed to the published version of this manuscript.

Funding: This research was made possible through internal funding by Viridien Group and the University of Twente as part of a joint research agreement.

Data Availability Statement: The data presented in this article are not readily available due to being part of an ongoing study. Requests to access the data should be directed to A.E.J. Botha and J. Fletcher.

Acknowledgments: The authors would like to thank Marc Smillie and Deepak Nair of NKT Photonics for providing access to their SuperK laser. The authors acknowledge Jonathan Franco Hempenius and Karin van den Nieuwenhuizen (GeoScience Laboratory, University of Twente) for their support in preparing the hardware and in the field campaign, and Junior Potgieter and Jeremie Messud (Viridien Group) for their general project support.

Conflicts of Interest: Authors Alfred Baines and Joe Fletcher are employed by Viridien Group. The remaining authors declare that this research was conducted in the absence of any commercial or financial relationships that could be construed as a potential conflict of interest.

Abbreviations

The following abbreviations are used in this manuscript:

CET	Central European Time
MNF	Minimum noise fraction
RGB	Red green blue
SWIR	Shortwave infrared
VNIR	Visible and near-infrared

References

1. Kirsch, M.; Mavroudi, M.; Thiele, S.; Lorenz, S.; Tusa, L.; Booysen, R.; Herrmann, E.; Fatihi, A.; Möckel, R.; Dittrich, T.; et al. Underground hyperspectral outcrop scanning for automated mine-face mapping: The lithium deposit of Zinnwald/Cínovec. *Photogramm. Rec.* **2023**, *38*, 408–429. [CrossRef]
2. Hunt, G. Near-infrared (1.3–2.4) μm spectra of alteration minerals—Potential for use in remote sensing. *Geophysics* **1977**, *44*, 1974–1986. [CrossRef]
3. Hecker, C.; van Ruitenbeek, F.; van der Werff, H.; Bakker, W.; Hewson, R.; van der Meer, F. Spectral absorption feature analysis for finding ore: A tutorial on using the method in geological remote sensing. *IEEE Geosci. Remote Sens. Mag.* **2019**, *7*, 51–71. [CrossRef]
4. Martino, R.; McCann, P.; Ray, R.; van der Ende, O. Trends in Underground Hard-Rock Mining for Gold and Base Metals. 2021. Available online: https://www.mckinsey.com/industries/metals-and-mining/our-insights/digging-deeper-trends-in-underground-hard-rock-mining-for-gold-and-base-metals (accessed on 1 November 2024).
5. Kurz, T.; Buckley, S.; Becker, J. Hyperspectral imaging: A novel geological mapping technique for subsurface construction sites. In Proceedings of the World Tunnel Congress: Surface Challenges—Underground Solutions, Bergen, Norway, 9–15 June 2017.
6. Manninen, A.; Kääriäinen, T.; Parviainen, T.; Buchter, S.; Heiliö, M.; Laurila, T. Long distance active hyperspectral sensing using high-power near-infrared supercontinuum light source. *Opt. Express* **2014**, *22*, 7172–7177. [CrossRef] [PubMed]
7. NKT Photonics. The SuperK FIANIUM Supercontinuum White Light Fibers Laser. Available online: https://www.nktphotonics.com/products/supercontinuum-white-light-lasers/superk-fianium/ (accessed on 1 November 2024).
8. Shao, H.; Chen, Y.; Yang, Z.; Jiang, C.; Li, W.; Wu, H.; Wen, Z.; Wang, S.; Puttnon, E.; Hyyppä, J. A 91-Channel Hyperspectral LiDAR for Coal/Rock Classification. *IEEE Geosci. Remote Sens. Lett.* **2020**, *17*, 1052–1056. [CrossRef]
9. Sun, H.; Wang, Z.; Chen, Y.; Tian, W.; He, W.; Wu, H.; Zhang, H.; Tang, L.; Jiang, C.; Jia, J.; et al. Preliminary verification of hyperspectral LiDAR covering VIS-NIR-SWIR used for objects classification. *Eur. J. Remote Sens.* **2022**, *55*, 291–303. [CrossRef]
10. Zhou, G.; Zhou, X.; Xie, Y.S.D.; Wang, L.; Hu, G.Y.M.; Liu, B.; Shang, W.; Gong, C.; Wang, C.; Huang, H.; et al. Design of supercontinuum laser hyperspectral light detection and ranging (LiDAR) (SCLaHS LiDAR). *Int. J. Remote Sens.* **2021**, *42*, 3731–3755. [CrossRef]
11. Chen, Y.; Jiang, C.; Hyyppä, J.; Qiu, S.; Wang, Z.; Tian, M.; Li, W.; Puttonen, E.; Zhou, H.; Feng, Z.; et al. Feasibility Study of Ore Classification Using Active Hyperspectral LiDAR. *IEEE Geosci. Remote Sens. Lett.* **2018**, *15*, 1785–1789. [CrossRef]
12. Nischan, M.; Joseph, R.; Libby, J.; Kerekes, J. Active spectral imaging. *Linc. Lab. J.* **2003**, *14*, 131–144.
13. Kääriäinen, T.; Jaanson, P.; Vaigu, A.; Mannila, R.; Manninen, A. Active Hyperspectral Sensor Based on MEMS Fabry-Pérot Interferometer. *Sensors* **2019**, *19*, 2192. [CrossRef] [PubMed]
14. Arribas, A.; Cunningham, C.; Rytuba, J.; Rye, R.; Kelly, W.; Podwysocki, M.; McKee, E.; Tosdal, R. Geology, geochronology, fluid inclusions, and isotope geochemistry of the Rodalquilar gold alunite deposit, Spain. *Econ. Geol.* **1995**, *90*, 795–822. [CrossRef]
15. Norsk Elektro Optikk (NEO). The HySpex Mjolnir Hyperspectral Imaging System. Available online: https://www.hyspex.com/hyspex-products/hyspex-mjolnir/hyspex-mjolnir-vs-620/ (accessed on 1 November 2024).
16. Zheng, X.; Yuan, Y.; Lu, X. Hyperspectral Image Denoising by Fusing the Selected Related Bands. *IEEE Trans. Geosci. Remote Sens.* **2019**, *57*, 2596–2609. [CrossRef]
17. Thiele, S.T.; Lorenz, S.; Kirsch, M.; Gloaguen, R. A Novel and Open-Source Illumination Correction for Hyperspectral Digital Outcrop Models. *IEEE Trans. Geosci. Remote Sens.* **2022**, *60*, 5511612. [CrossRef]

Disclaimer/Publisher's Note: The statements, opinions and data contained in all publications are solely those of the individual author(s) and contributor(s) and not of MDPI and/or the editor(s). MDPI and/or the editor(s) disclaim responsibility for any injury to people or property resulting from any ideas, methods, instructions or products referred to in the content.